

Stretchable electromagnetic interference shielding and antenna for wireless strain sensing by anisotropic micron-steel-wire based conductive elastomers

Xiaoyu Hu(胡晓宇), Linlin Mou(牟琳琳), and Zunfeng Liu(刘遵峰)†

Citation: Chin. Phys. B, 2021, 30 (**1**): 018401. DOI: 10.1088/1674-1056/abc2b3
Journal homepage: http://cpb.iphy.ac.cn; http://iopscience.iop.org/cpb

What follows is a list of articles you may be interested in

Dual-polarized lens antenna based on multimode metasurfaces

Hao-Fang Wang(王浩放), Zheng-Bin Wang(王正斌), Yong Cheng(程勇), Ye-Rong Zhang(张业荣)
Chin. Phys. B, 2018, 27 (**11**): 118401. DOI: 10.1088/1674-1056/27/11/118401

Correction of failure in antenna array using matrix pencil technique

S U Khan, M K A Rahim
Chin. Phys. B, 2017, 26 (**6**): 068401. DOI: 10.1088/1674-1056/26/6/068401

An ultra-wideband pattern reconfigurable antenna based on graphene coating

YanNan Jiang(姜彦南), Rui Yuan(袁锐), Xi Gao(高喜), Jiao Wang(王娇), SiMin Li(李思敏), Yi-Yu Lin(林诒玉)
Chin. Phys. B, 2016, 25 (**11**): 118402. DOI: 10.1088/1674-1056/25/11/118402

Metallic spherical anechoic chamber for antenna pattern measurement

Ali Farahbakhsh, Mohammad Khalaj-Amirhosseini
Chin. Phys. B, 2016, 25 (**8**): 088401. DOI: 10.1088/1674-1056/25/8/088401

Wideband dipole antenna with inter-digital capacitor

Xiong Han, Hong Jin-Song, Jin Da-Lin
Chin. Phys. B, 2013, 22 (**4**): 048401. DOI: 10.1088/1674-1056/22/4/048401

Stretchable electromagnetic interference shielding and antenna for wireless strain sensing by anisotropic micron-steel-wire based conductive elastomers*

Xiaoyu Hu(胡晓宇), Linlin Mou(牟琳琳), and Zunfeng Liu(刘遵峰)†

State Key Laboratory of Medicinal Chemical Biology, College of Pharmacy and Chemistry, and Key Laboratory of Functional Polymer Materials, Nankai University, Tianjin 300071, China

(Received 9 September 2020; revised manuscript received 20 October 2020; accepted manuscript online 20 October 2020)

We prepare stretchable elastic electromagnetic interference (EMI) shielding and stretchable antenna for wireless strain sensing using an elastic composite comprising commercial steel wool as a conducting element. The prepared elastic conductor shows anisotropic electrical properties in response to the external force. In the stretchable range, the electrical resistance abnormally decreases with the increase of tensile deformation. The EMI shielding effectiveness of the elastic conductor can reach above −30 dB under 80% tensile strain. The resonance frequency of the dipole antenna prepared by the elastic conductor is linearly correlated with the tensile strain, which can be used as a wireless strain sensor. The transmission efficiency is stable at about −15 dB when stretched to 50% strain, with attenuation less than 5%. The current research provides an effective solution for stretchable EMI shielding and wireless strain sensing integrated with signal transmission by an antenna.

Keywords: conductive elastomer, electromagnetic shielding, dipole antenna, strain sensor

PACS: 84.32.Ff, 84.40.Ba, 81.05.Ni, 07.50.–e **DOI:** 10.1088/1674-1056/abc2b3

1. Introduction

With the development of wearable electronic devices, various stretchable devices have been developed, including elastic conductors,[1] flexible sensors,[2] flexible power supplies,[3] and wearable electromagnetic protection devices.[4] For example, stretchable electromagnetic devices show important applications in wearable electronics for protection and signal transmission. Elastic electromagnetic interference (EMI) shielding can protect persons against electromagnetic pollution; and stretchable antenna can transmit electromagnetic signals wirelessly under deformation. Different strategies have been developed to realize stretchable EMI shielding and stretchable antenna. Stretchable EMI shielding devices have been realized using carbon nanotube (CNT) infiltrated foams,[4–6] buckled silver nanowire (AgNW) multi-layers,[7] and buckled Fe_3O_4-CNT elastomer layers.[8] Stretchable antennas have been fabricated using a wavy AgNW network,[9] EGaIn-polydimethylsiloxane (PDMS),[10] and *in situ* generated silver nanoparticles (AgNPs).[11] Although great progress has been achieved, it is still a challenge to improve the stability of stretchable EMI shielding effectiveness at large deformation and to maintain the stability of emission efficiency of the signal for wireless strain sensing via stretchable antenna using a cost-effective conductive composite.

Elastic conductors are the basic components for stretchable EMI shielding and stretchable antenna devices. Therefore, to develop elastic conductors with non-decayed electric conductance under large deformation is required for high-performance stretchable EMI and stretchable antenna devices; and a low cost, simple preparation method to prepare elastic conductors is necessary for ease of mass production and commercialization. The microscopic mechanism of electric conduction determines that the conductor itself has a certain rigidity (e.g., metals). However, stretchability comes from the variability of the internal structure of a material, so stretchability and conductivity are generally two contradictory material properties. This problem can be solved using different strategies by material selection and structural design.

Researchers have found some nanomaterials that have inherently good stretchability and conductivity, such as single-walled carbon nanotubes,[2,12] graphene,[13] ionic gels,[14] conducting polymers[15] to meet the needs of some applications in flexible and stretchable electronics. A second strategy is to mix conductive fillers into the polymer matrix to make a composite, including carbon nanomaterials,[16] metals such as silver nanowires,[17,18] silver micro-flakes,[19] and silver nano-particles,[20] copper,[21] etc. The prepared elastic conductors always show increased electrical resistance un-

*Project supported by the State Key Development Program for Basic Research of China (Grant Nos. 2016YFA0200200 and 2017YFB0307001), the National Natural Science Foundation of China (Grant Nos. 51973093, U1533122, and 51773094), and the Natural Science Foundation of Tianjin, China (Grant No. 18JCZDJC36800).

†Corresponding author. E-mail: liuzunfeng@nankai.edu.cn

© 2021 Chinese Physical Society and IOP Publishing Ltd

der stretching due to the disconnection between conductive fillers. Compared to the simple blending of conductive components and elastic components, the introduction of buckling,[22] spirals,[23] rigid-island structures,[24] serpentine[25] can simultaneously improve the stretchability and conductivity of the elastic conductor. These structures are always realized in a thin conductive layer, and therefore it is difficult to prepare a bulk composite. Moreover, the high cost of materials and fabrication procedures is a limit for practical applications in the aspects of mass production and commercialization. Steel wool is made of anisotropic aligned micro-steel wires that show good conductivity with a large abundance of industrial supplies, which has been proved to be suitable for preparing elastic conductors with non-decayed conductance during large deformation.[26] Up to date, stretchable EMI shielding and stretchable antenna devices have not been developed using anisotropic micron-steel-wire composites.

In this paper, stretchable EMI shielding and stretchable antenna devices are prepared using commercially available steel wool as the conductive material and using plasticized poly (styrene-hydrogenated butadiene-styrene, i.e., SEBS) as the elastic matrix to prepare a conductive composite. The anisotropic mechanical and electrical properties of the steel wool-based elastic conductors are systematically studied under different external stresses. The comparison of resistance changes and expenses per mass with different conductive fillers shows that the steel wool-based elastic conductor presents the unique advantages in stable electrical properties at a low cost. The stretchable EMI shielding performances under different strains and the stretchable dipole antenna for wireless strain sensing based on steel wool-based elastic conductors are investigated.

2. Steel wool-based elastic conductive composites

2.1. Sample fabrication

In this article, commercialized steel wool (Bon Star Co., Ltd., Model 0000) is used as the conducting fillers for constructing the elastic conductors. Steel wool is composed of short fibers with a length distribution ranging from 3 mm to 5 cm and a diameter of about 25 μm. Although these metal fibers are slightly curved, their arrangement has high anisotropy and they contact with each other closely, as shown in the optical photo in Fig. 1(a). These short fibers have a certain degree of anisotropy and stretchability. The plasticized SEBS rubber was used as the elastic material, with the preparation method shown in Fig. 1(b). SEBS rubber powder (U.S. Kraton Company, G-1651) and plasticizer liquid paraffin (Chemical Market Co., Ltd., No. 5) were mixed uniformly with a mass ratio of 1:5, and then heated to 200 °C using the graphite electric heating plate (Lichen Technology Co., Ltd., DB-1EF). The thickness of the sample was kept below 5 mm to ensure uniform temperature distribution during heating. The rubber powder was well dispersed in the plasticizer by mechanical mixing. The molten blend of the above mixture was then cast into steel wool, and the mold was used for shaping and cutting to fix the shape of the steel wool-based conductive composites. The elastic conductor in this article was obtained after the sample was slowly cooled down to room temperature. The volume fraction of the steel wool in the elastic conductor can be adjusted by controlling the size of the mold. In the present experiments, the volume fraction value was calculated to be about 6.7%. The estimated costs for conductive fillers used per volume of the elastic conductors were compared, with data shown in Table S1 and illustrated in Fig. 2. The steel wool-based elastic conductors were cost-effective while providing adequate conductance among various kinds of conductive fillers.

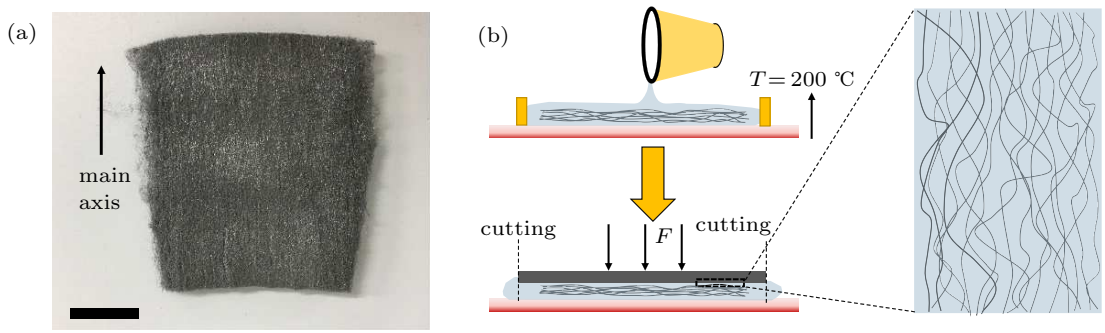


Fig. 1. Preparation of steel-wool based conductive elastomers. (a) The optical photo of the steel-wool, scale bar: 1 cm. (b) Schematic illustrations for the sample preparation of conductive elastic composites composed of steel-wool and elastomer.

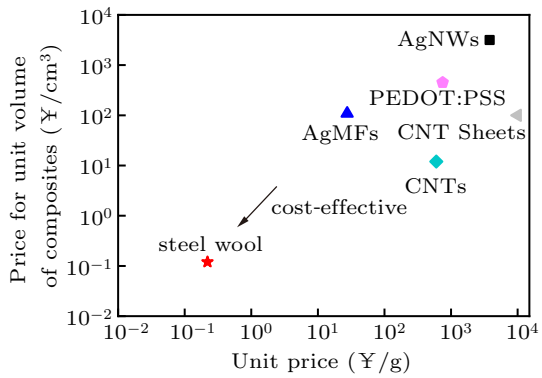


Fig. 2. Comparison of cost assessment of different conductive fillers for elastic conductor composites at the lab scale.

2.2. Mechanical properties of anisotropic steel wool elastic conductors

Two parameters describing the morphology of the steel wool in the elastic conductor, the orientation degree ϕ, and the theoretical stretchability along the main axis ξ, where the main axis refers to the average direction of micron steel wire in the composite. It is defined that the orientation degree is the number-average value of the square of the cosine value of the angle from the direction of the wire to the main axis of steel wool in a certain field of view. Similarly, the actual length of the wire is greater than the line distance along the main axis. Thus, the number average value of the increased ratio of the above two parameters is defined as the theoretical stretchability. The calculation method is shown in Fig. 3(a). Assume that θ_i is the angle between the main axis and the line started at the starting point and ended at the ending point of the i^{th} wire, d_i is the projected length of the line between the starting point and the ending point in the main axis direction, and l_i is the actual length of the wire between these two points. Then the orientation degree ϕ and theoretical stretchability ξ can be calculated by

$$\phi = \frac{\sum_i n_i \cos^2\theta_i}{\sum_i n_i} \times 100\%, \tag{1}$$

$$\xi = \left(\frac{\sum_i n_i l_i/d_i}{\sum_i n_i} - 1\right) \times 100\%, \tag{2}$$

where n_i is the number corresponding to the i^{th} wire.

According to the results shown in Table S2, we can find that before stretching, the values of ϕ and ξ for steel wool are 85.2%±9.80% and 45.3%±21.1%, respectively, showing relatively high anisotropy and moderate stretchability. Therefore, its mechanical properties are expected to be anisotropic. As shown in Fig. 3(b), as the stretching direction of the sample is parallel to the main axis of the steel wool, Young's modulus of the elastic conductor is 0.25 MPa, and as the tensile strain is perpendicular to the main axis, Young's modulus decreases to 0.125 MPa.

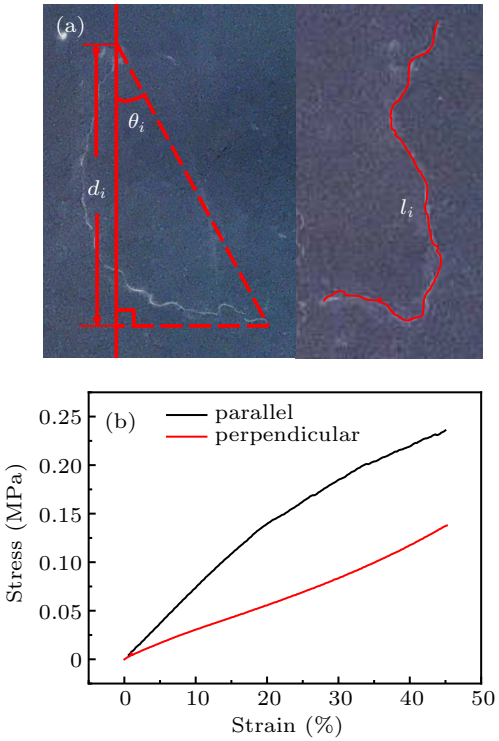


Fig. 3. Structural analysis and mechanical properties of steel-wool based conductive elastomers. (a) Schematic illustration for the calculation of the degree of orientation and theoretical stretchability. (b) The stress-strain curves of conductive elastomers upon stretching in the directions parallel and perpendicular to the main axis.

2.3. Electrical properties of anisotropic steel wool elastic conductors under strain

Similarly, the electrical properties of the steel wool elastic conductors also show obvious anisotropy. Considering that the resistance of steel wool is very small (Figs. 4(a) and 4(b)), the resistance must be measured by a digital source meter (Keithley 2400, USA) using the four-wire method. It can be seen from Fig. 4(c) that as the test ends are at the two ends of the main axis of the steel wool, the initial composite conductivity reaches 170 S/m. While the connection direction of the positive and negative electrodes for electrical testing is perpendicular to the main axis of the steel wool, the initial conductivity drops to 55 S/m, about 1/3 of that in the main axis direction. We then stretched the elastic conductors and measured the resistance at both ends of the elastic conductor in the stretched direction. It is found that the conductivity of the elastic conductor increases as the tensile strain increases regardless of the stretching direction. Figures 4(c) and 4(d) show that when the testing direction is parallel to the main axis of the steel wool, the electrical conductivity increases from 170 S/m to a maximum value of 200 S/m at 13% tensile strain, and at the same time, the resistance decreases by 11%. As the testing direction is perpendicular to the main axis of the steel wool, the conductivity increases from 55 S/m to 85 S/m at 48% tensile strain, and at the same time, the resistance decreases by 36%. The resistance changes under cycling tensile strain of 40% are illustrated in Fig. S1, with the stretching rate of 0.3 mm/s. The

resistance change becomes stable after cycles of training during the investigated 150 cycles when the stretching direction is perpendicular to the main axis of the steel wool. The encapsulation of SEBS rubber to the metal wool is assumed to be essential for improved cyclic endurance.

Generally, as the tensile strain increases, the resistance of the elastic conductor gradually increases. This is due to the fact that the connection between the conductive fillers decreases upon stretching or the distance between conductive fillers increases. On the contrary, the resistance of the steel-wool elastic conductor in this work decreases with an increase of the tensile strain. This is because the stretching process also causes the metal wool to be squeezed in the width and thickness directions, which increases the contact points between the conductive fibers and reduces the average length of the conductive path. Therefore, we observed resistance decrease upon stretching. A similar phenomenon was also reported in some conductive elastomers using tricot weave as a polymer matrix.[1,27]

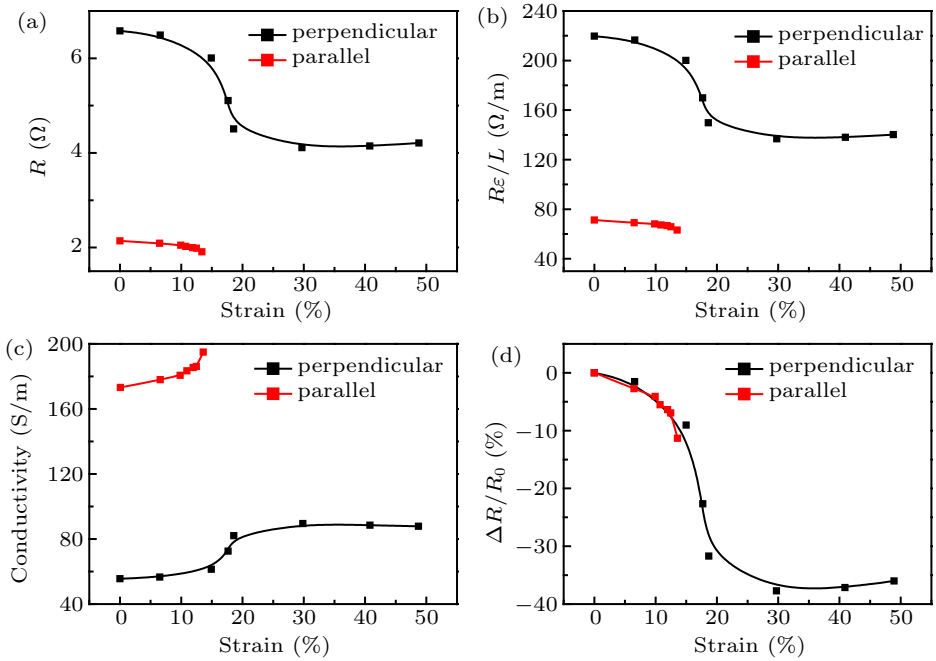


Fig. 4. Electrical properties of steel-wool conductive elastomers under stretching. (a) Resistance change, (b) resistance change per initial length, (c) electrical conductivity, and (d) the percent resistance change to the initial resistance ($\Delta R/R_0$).

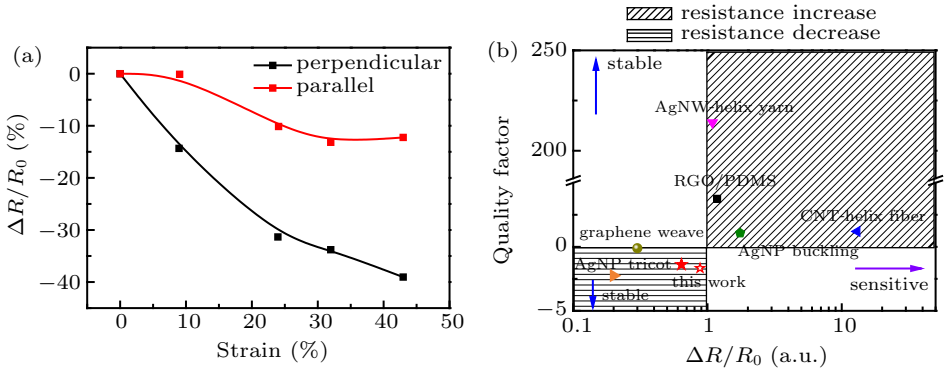


Fig. 5. Electrical properties of steel-wool composites under compressing and stretching. (a) The percent resistance change ($\Delta R/R_0$) of steel wool conductive elastomer under compressing. (b) Comparison of quality factor and resistance change for both stretch-induced resistance increase and stretch-induced resistance decrease for different conductive elastomers in this work and in literature, with data shown in Table S3.

The resistance changes in the directions perpendicular and parallel to the main axis of the steel wool under different compressive strains are then studied. The elastic conductor is sandwiched between two splints, with a certain pressing load applied on the top splint, so that the pressure can be evenly distributed on the sample. As shown in Fig. 5, as the compressive deformation increases to 40%, the resistance in the direction perpendicular to the main axis decreases by 40%, while the resistance parallel to the main axis decreases by about 10%. This is because the mutual contact between micron steel wires in the steel wool increases upon compressing. As the steel wool is subjected to surface pressure, the increase in the contacting area between the overlapping metal wires facilitates the electron conduction in the direction perpendicular

to the main axis, resulting in greater resistance decrease in the perpendicular direction as compared to the alignment direction of the steel wire in the steel wool. Such stretch-induced resistance decrease shows a negative sign of the quality factor (the percentage strain change divided by the percent resistance change) upon stretching up to 50% tensile strain (Fig. 5(b) and Table S3).

3. Steel wool elastic conductor for EMI shielding under strain

3.1. Methods for EMI shielding under strain

Electromagnetic wave presents in the environment and can also be emitted by electronic devices, therefore protection against the radiation of electromagnetic waves is important for both persons and wearable devices using a stretchable EMI shielding device. In this section, we test the EMI shielding properties of the elastic steel wool composite under different strains. The basic mechanism for EMI shielding is as follows. The incident electromagnetic wave can be transmitted, absorbed, or reflected when interacting with the material. Suppose that the emitted electromagnetic wave power is P_{I}, and the powers of reflected and transmitted electromagnetic wave after interacting with the sample are P_{R} and P_{T}, respectively. The reflected signal S_{11} and transmission signal S_{12}, which can be measured by the network analyzer, can be calculated by

$$|S_{11}| = \sqrt{\frac{P_{\mathrm{R}}}{P_{\mathrm{I}}}}, \tag{3}$$

$$|S_{12}| = \sqrt{\frac{P_T}{P_{\mathrm{I}}}}, \tag{4}$$

$$\mathrm{SE_R} = -10\log(1-|S_{11}|^2). \tag{5}$$

EMI shielding will produce return loss (reflection power, $\mathrm{SE_R}$), which is an important parameter to measure the shielding effectiveness of electromagnetic waves, and its calculation method is shown by Eq. (5).[5]

The range of the electromagnetic wave studied in this paper is 8–12 GHz, and the test method is the waveguide method. The schematic diagram of the device is shown in Fig. 6(a). The antennas on both sides of the sample are used to detect S_{11} and S_{12}, respectively. The elastic conductor samples with length, width, and thickness of 40 cm, 40 cm, and 5 mm are placed between the two antennas for EMI shielding measurements. The samples are uniaxially stretched perpendicular to the main axis of the steel wool to different strains during testing for evaluation of EMI shielding effectiveness of the elastic conductor.

3.2. EMI shielding performance of the steel wool elastic composite under strain

The effectiveness of electromagnetic shielding has a great relationship with the integrity of the conductive network for conductors. The electromagnetic shielding effectiveness of the elastic conductor in this work mainly comes from the reflection of electromagnetic waves. Figure 6(b) shows that in the 8–12 GHz test band, the return loss of the sample at 0% strain is above 38 dB, and increases slightly for all the band frequency range at 20% strain. This should originate from the resistance decrease observed during uniaxial stretching as shown in Fig. 4(a). At 40% strain, the EMI shielding effectiveness almost equals that at 0% strain for the 8–12 GHz test range. At 60% and 80% strain, the EMI shielding effectiveness is above 36 and 35 dB. The stable EMI shielding effectiveness at different strains should be ascribed to the non-decayed resistance under stretching. As shown in Section 2.3, because the elastic conductor still maintains a low resistance after being stretched, even lower than the initial resistance, so the conductivity and EMI shielding performance keep stable in the stretched state. At the same time, the general conductive materials are prone to defect during the stretching process, which may be the reason for slightly reduced EMI shielding effectiveness observed at high strains.

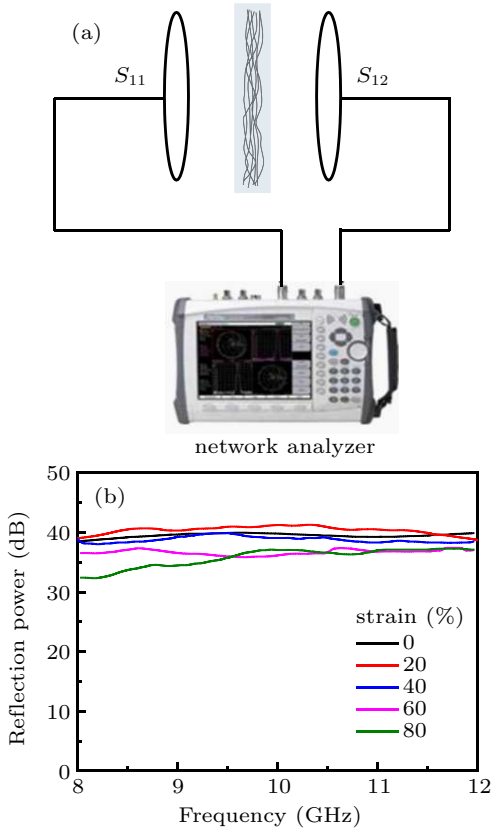


Fig. 6. Stretchable EMI shielding by steel-wool conductive elastomers. (a) Schematic illustrations of the devices for EMI shielding measurements by the waveguide method. (b) The EMI shielding effectiveness of the conductive elastomers in the range of 8–12 GHz under uniaxial stretching.

4. Steel wool elastic conductor for wireless strain sensor based on stretchable dipole antenna

4.1. Stretchable antenna for wireless strain sensor

The stretchable strain sensor is required in wearable electronics for monitoring the movement of a person or a soft robot to obtain the real-time behavior information of a person or the robot. In addition, such information has to transmit wirelessly to the control center or the data collecting devices. The resonant frequency of an ideal dipole antenna can be expressed by[11]

$$f = \frac{143}{l \cdot \varepsilon_{\text{eff}}^{0.5}}, \tag{6}$$

where l refers to the length of the conductive arm in meters, and ε_{eff} represents the effective relative permittivity of the medium around the conductor, which is a constant value. It can be inferred that the resonance frequency of a dipole antenna is dependent on its length. Therefore, measuring the stretchable antenna's resonance frequency may give information of strain. This single device would combine two functions including strain sensing and wireless signal transmission. Here, a linear change of the resonance frequency with strain and stable return loss of the emitted signal is highly desired. The low cost, ease of preparation, and non-decayed electric properties of the steel wool elastic composite encourage us to prepare a stretchable antenna for wireless strain sensing.

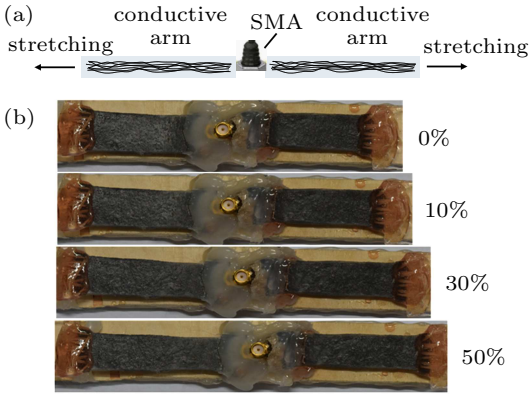


Fig. 7. Stretchable dipole antenna containing steel-wool based conductive elastomers. (a) Schematic illustrations of the antenna. (b) Optical photos of the antenna under mechanical stretch at different tensile strains.

The antenna prepared in this work is a dipole antenna, which consists of a testing SMA port and two collinear conductor arms with the same length, but opposite directions connected to the port (Fig. 7(a)). The conductor's arm is 6.8 cm long, 1.5 cm wide, and 0.5 cm thick. The preparation procedures of the conductor's arm are the same as those of the elastic conductor above. Note that the main axis of the steel wool is perpendicular to the length direction of the conductor's arm. One end of the two conductor arms is connected to the two electrodes of the SMA port. To ensure the stability of the interfacial area, the connection part is connected to a copper wire, encapsulated, and fixed with conductive glue and epoxy resin in turn. The other end is connected with an insulating handle for stretching. During testing, the SMA port is connected with the coaxial cable of the network analyzer (Keysight, E8363C, USA), and the antenna is fixed on the stretchable bracket to facilitate the tensile deformation of the conductor arms of the dipole antenna (Fig. 7(b)).

4.2. Performance of stretchable dipole antenna using steel-wool based conductive elastomers

The return loss of the antenna in the range of 0.1–1.8 GHz under different tensile strains is recorded by a network analyzer, with results shown in Fig. 8(a). The peak values of return loss are −15.9 dB and −15.47 dB under the original length and tensile strain of 50%, respectively. It is indicated that the antenna's radiation capability is almost unaffected by the tensile deformation, which is also due to the negligible loss of electrical conductance of the two arms during stretching. Then, Ansys HFSS software is used to simulate the return loss curve of the dipole antenna. According to the data mentioned above, the shape and conductivity of the dipole antenna after stretching are adjusted before simulation. The results are shown by the dotted line in Fig. 8(a), and the curve peak position and return loss power of theoretical simulation results are consistent with those of the actual measured data. For example, when the tensile strain is 50%, the return loss peak value of the simulated curve is −15.91 dB, and the resonance frequency is 0.68 GHz, which are in good agreement with the actual measured data.

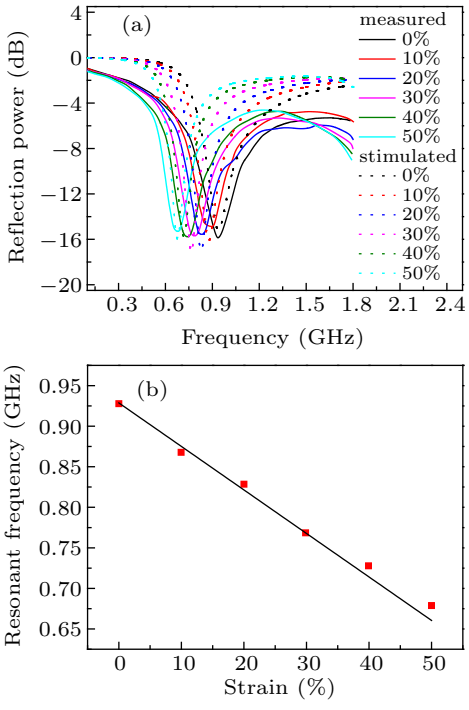


Fig. 8. Performance of stretchable dipole antenna. (a) Reflection power in the range of 0.1–1.8 GHz. (b) Resonant frequency under different tensile strains.

It can be seen that as the tensile strain increases, the resonant frequency of the antenna shifts to the low-frequency side, which is almost linearly correlated with the tensile strain for the tested range (Fig. 8(b)). In the range shown in Fig. 8(b), the antenna's resonance frequency and tensile strain are approximately in a negative linear relationship. As the tensile strain increases from 0 to 50%, the resonance frequency quasi-linearly decreases from 0.928 GHz to 0.679 GHz. The almost linear relationship between resonance frequency and tensile strains, with negligible signal attenuation during tensile deformation, make it a good choice for wireless strain sensing, by measuring the resonance frequency of the stretchable dipole antenna wirelessly using a receiver device. Furthermore, with simulation results obtained from HFSS, the length of the conductive arm of the dipole antenna can be changed (e.g., 1.0 cm), while keeping the linear response of resonance frequency on the tensile strains (Fig. S2). Thus, the dipole antenna can be used for wireless strain sensor without space limitations theoretically, by providing a receiver that can respond to the corresponding frequency range.

Furthermore, HFSS software was used to simulate the far-field radiation of the dipole antenna. The three-dimensional gain total data of the antenna in the original length and after 50% stretch are shown in Figs. 9(a) and 9(b). In the direction parallel to that of the conductive arm (y-axis), the antenna shows minimum radiation. For a more intuitive comparison, Figs. 9(c) and 9(d) show the projections on the $\boldsymbol{E}$ plane and the $\boldsymbol{H}$ plane of the three-dimensional gain diagrams of the antenna under different tensile strains. It can be seen that after stretching the dipole antenna, the radiation gain does not change significantly in both $\boldsymbol{E}$ and $\boldsymbol{H}$ planes. There is only a slight increase in the orientation of the projection on the $\boldsymbol{H}$ plane due to the antenna length change in the stretching direction.

The performances of the EMI shielding effectiveness and reflection power for stretchable EMI shielding materials and antennas after tensile stretch are compared (Fig. 10, Table S4). To evaluate the signal stability in different reports, the stability coefficient σ is defined as the performance value at the stretched state divided by the performance value at 0% tensile strain and then multiplied by the square of the corresponding tensile strain value, i.e.,

$$\sigma = \frac{10^{-0.1\mathrm{SE}_{\mathrm{R},\varepsilon}}}{10^{-0.1\mathrm{SE}_{\mathrm{R},0}}} \cdot \varepsilon^2, \tag{7}$$

where $\mathrm{SE}_{\mathrm{R},0}$ and $\mathrm{SE}_{\mathrm{R},\varepsilon}$ refer to the reflection power for the composites that are not stretched or at a tensile strain ε, respectively, for EMI shielding or dipole antenna. It is seen that the steel-wool based conductors can keep stable performance upon tensile deformation, making them a promising choice for further applications in electromagnetic stretchable electronics.

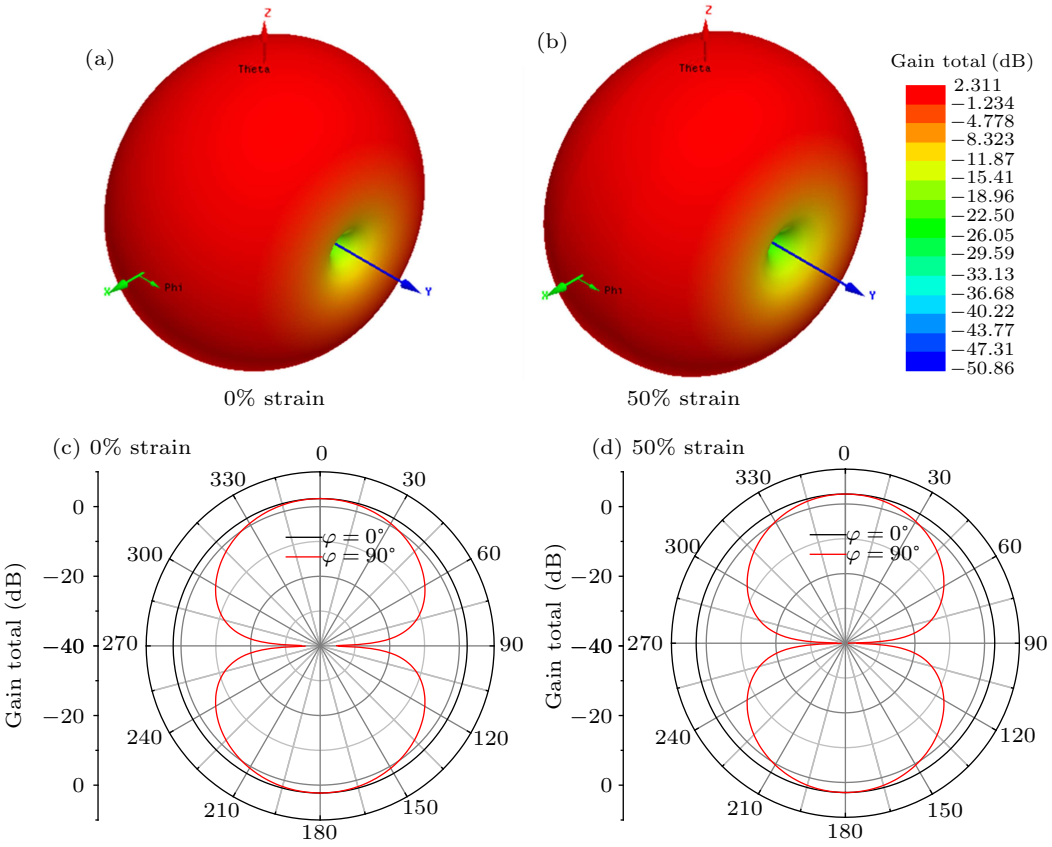


Fig. 9. Stimulated 3D radiation patterns of the stretchable dipole antenna before and after tensile strain. (a) The 3D radiation patterns at 0% strain. (b) The 3D radiation patterns under 50% tensile strain. (c) The radiation patterns in $\boldsymbol{E}$ and $\boldsymbol{H}$ planes at 0% strain. (d) The radiation patterns in $\boldsymbol{E}$ and $\boldsymbol{H}$ planes at 50% strain.

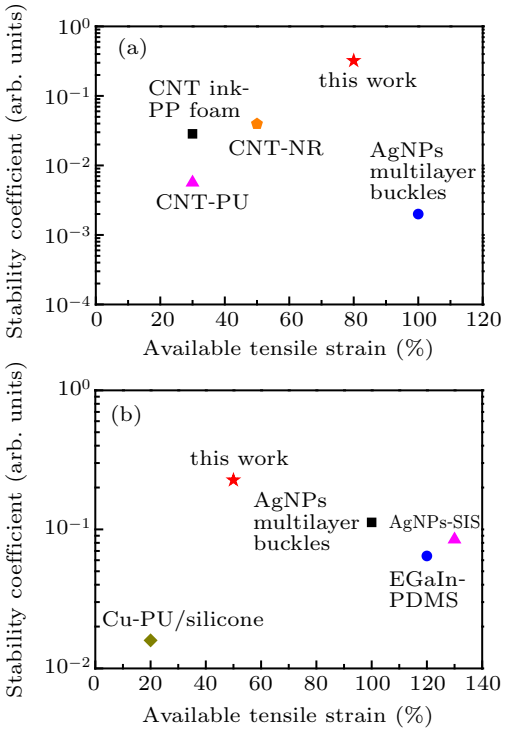


Fig. 10. Comparison of (a) EMI shielding effectiveness for stretchable EMI shielding and (b) return loss for the stretchable antenna.

5. Conclusions and perspectives

In summary, a low-cost, easy fabrication method has been developed to construct stretchable EMI shielding and stretchable antenna devices for wireless strain sensing, using steel wool mixed with a molten liquid of plasticized SEBS rubber. Because the arrangement of the short fibers in steel wool is both anisotropic and elastic, more contact points of this kind of steel wool-based elastic conductor will generate as the tensile strain increases, causing the non-decayed resistance under stretching. It avoids the problem of stretch-induced conductivity attenuation, which is observed for general elastic conductors. Therefore, this kind of elastic conductor can be used as an ideal candidate for stretchable electromagnetic electronic devices such as stretchable EMI shielding and antennas. Compared with previous reports, the steel-wool based stretchable EMI shielding and antennas provide superior stability of emission efficiency, as well as cost-effectiveness and ease of mass fabrication. The resonance frequency of the dipole antenna has an approximately linear relationship with tensile strains, making it a preferred choice for wireless strain sensing. This work provides new inspirations for the structural design of elastic electromagnetic devices.

References

[1] Lee Y H, Kim Y, Lee T I, Lee I, Shin J, Lee H S, Kim T S and Choi J W 2015 *ACS Nano* **9** 12214

[2] Lipomi D J, Vosgueritchian M, Tee B C K, Hellstrom S L, Lee J A, Fox C H and Bao Z 2011 *Nat. Nanotechnol.* **6** 788

[3] Parida K, Thangavel G, Cai G, Zhou X, Park S, Xiong J and Lee P S 2019 *Nat. Commun.* **10** 2158

[4] Jia L C, Yan D X, Yang Y C, Zhou D, Cui C H, Bianco E, Lou J, Vajtai R, Li B, Ajayan P M and Li Z M 2017 *Adv. Mater. Technol.* **2** 1700078

[5] Huang K, Chen M, He G, Hu X, He W, Zhou X, Huang Y and Liu Z 2020 *Carbon* **157** 466

[6] He W, Zhang R, Cheng Y, Zhang C, Zhou X, Liu Z, Hu X, Liu Z, Sun J, Wang Y, Qian D and Liu Z 2020 *Sci. Chin.-Mater.* **63** 1318

[7] Liu Z S, Wan F Y, Mou L L, de Andrade M J, Qian D, Wang R, Yin S G, Li K, Chen H, An B G, Hu Z Z, Wang H Z, Zhu M F, Fang S L and Liu Z F 2019 *Adv. Electron. Mater.* **5** 1800817

[8] Shao Y, Li J, Lu W, Xiao J Q, Qiu Y and Chou T-W 2018 *ACS Appl. Nano Mater.* **1** 2227

[9] Kim B S, Shin K Y, Pyo J B, Lee J, Son J G, Lee S S and Park J H 2016 *ACS Appl. Mater. Interfaces* **8** 2582

[10] Kubo M, Li X, Kim C, Hashimoto M, Wiley B J, Ham D and Whitesides G M 2010 *Adv. Mater.* **22** 2749

[11] Park M, Im J, Shin M, Min Y, Park J, Cho H, Park S, Shim M B, Jeon S, Chung D Y, Bae J, Park J, Jeong U and Kim K 2012 *Nat. Nanotechnol.* **7** 803

[12] Fan Q, Zhang Q, Zhou W, Yang F, Zhang N, Xiao S, Gu X, Xiao Z, Chen H, Wang Y, Liu H and Zhou W 2017 *Chin. Phys. B* **26** 028801

[13] Qin M M, Ji W, Feng Y Y and Feng W 2014 *Chin. Phys. B* **23** 028103

[14] Kim C C, Lee H H, Oh K H and Sun J Y 2016 *Science* **353** 682

[15] Wang Y, Zhu C, Pfattner R, Yan H, Jin L, Chen S, Molina-Lopez F, Lissel F, Liu J, Rabiah N I, Chen Z, Chung J W, Linder C, Toney M F, Murmann B and Bao Z 2017 *Sci. Adv.* **3** e1602076

[16] Sekitani T, Noguchi Y, Hata K, Fukushima T, Aida T and Someya T 2008 *Science* **321** 1468

[17] Kim B S, Pyo J B, Son J G, Zi G, Lee S-S, Park J H and Lee J 2017 *ACS Appl. Mater. Interfaces* **9** 10865

[18] He S, Zhang X, Yang B, Xu X, Chen H and Zhou C 2017 *Chin. Phys. B* **26** 078103

[19] Kim S H, Seo H, Kang J, Hong J, Seong D, Kim H J, Kim J, Mun J, Youn I, Kim J, Kim Y C, Seok H K, Lee C, Tok J B, Bao Z and Son D 2019 *ACS Nano* **13** 6531

[20] Hu M, Cai X, Guo Q, Bian B, Zhang T and Yang J 2016 *ACS Nano* **10** 396

[21] Li C, Gong X, Tang L, Zhang K, Luo J, Ling L, Pu J, Li T, Li M and Yao Y 2015 *J. Mater. Chem. C* **3** 6178

[22] Kim B S, Kwon H, Kwon H J, Pyo J B, Oh J, Hong S Y, Park J H, Char K, Ha J S, Son J G and Lee S S 2020 *Adv. Funct. Mater.* **30** 1910214

[23] Cheng Y, Wang R R, Chan K H, Lu X, Sun J and Ho G W 2018 *ACS Nano* **12** 3898

[24] Kim Y, Jun S, Ju B K and Kim J W 2017 *ACS Appl. Mater. Interfaces* **9** 7505

[25] Li C F, Li W L, Zhang H, Liu J T, Yang Y, Li L Y, Gao Y, Liu Z Q and Suganuma K 2019 *ACS Appl. Mater. Interfaces* **11** 3231

[26] Lessing J, Morin S A, Keplinger C, Tayi A S and Whitesides G M 2015 *Adv. Funct. Mater.* **25** 1418

[27] Yang Z, Pang Y, Han X L, Yang Y, Ling J, Jian M, Zhang Y, Yang Y and Ren T L 2018 *ACS Nano* **12** 9134